Implications of layered double hydroxides assembled biochar composite in adsorptive removal of contaminants: Current status and future perspectives

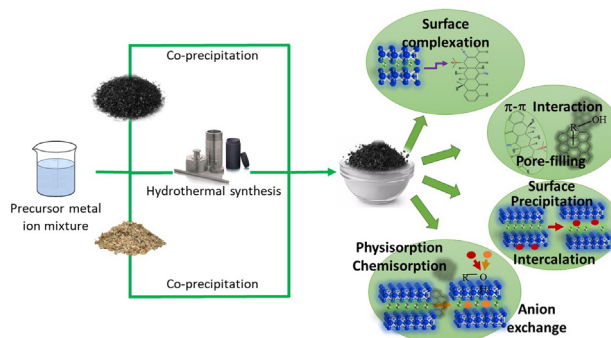Meththika Vithanage [a,*], Ahmed Ashiq [a], Sammani Ramanayaka [a], Amit Bhatnagar [b,*]

[a] Ecosphere Resilience Research Center, Faculty of Applied Sciences, University of Sri Jayewardenepura, Nugegoda 10250, Sri Lanka
[b] Department of Environmental and Biological Sciences, University of Eastern Finland, P. O. Box 1627, FI-70211 Kuopio, Finland

HIGHLIGHTS

- Layered double hydroxides are assembled with biochar to produce LDH-BC composite.
- This is the first review on LDH-BC composite for contaminant remediation.
- LDH-BC composites are widely used in adsorptive remediation of contaminants.
- Adsorption capacities are high but partition coefficient is low for many composites.

GRAPHICAL ABSTRACT

ARTICLE INFO

ABSTRACT

In recent years, biochar composites have received considerable attention for environmental applications. This paper reviews the current state of research on Layered Double Hydroxides (LDHs) tailored biochar composites in terms of their synthesis methods, characteristics, and their use as adsorbents for the removal of various pollutants from water, highlighting and discussing the key advancement in this area. The adsorption potential of LDHs-biochar composites for different inorganic and organic contaminants, important factors affecting composites' properties and the adsorption process, and the mechanisms involved in adsorption are discussed in this review. Though the adsorption capacities are high for the composites studied, partition coefficient which suggest the performance of composites remain low for most adsorbents. Despite the recent progress in the synthesis of LDHs-biochar composites, further research is needed to improve the performance of composites for different classes of aquatic pollutants, and to test their applicability in pilot-scale with real wastewater under real environmental conditions.

1. Introduction

Biochar is a carbon-rich organic material, produced by pyrolysis of organic materials, and has various applications such as soil conditioning, promoting microbiological activity, increasing water holding capacity enhancing nutrient availability in soils and removal of contaminants

from water (Ahmad et al., 2014; Mandal et al., 2020; Peiris et al., 2019). Biochars' characteristics are mainly governed by the feedstock type, synthesis procedures and pyrolyzing conditions. Modifications of biochar are generally essential to improve its performance (Premarathna et al., 2019b; Rajapaksha et al., 2016). Among different applications of biochar, water treatment has received wide attention as biochar has the potential to remove a wide range of contaminants, including toxic metals, nutrients, pharmaceuticals, personal care products, agrochemicals, and persistent organic compounds (Peiris et al., 2017; Vithanage et al., 2017). Use of biochar over activated carbon (AC) is preferred mainly due to its close similarities with AC, though biochar has a lesser surface area and porosity and less energy requirement than AC (Premarathna et al., 2019b). Different modifications of biochar have been suggested in order to improve its performance towards contaminants removal from water.

Among numerous modification methods, biochar composites were studied in detail, mainly due to the cost-effectiveness and improved performance (Premarathna et al., 2019b; Rajapaksha et al., 2016). Designer biochars are blended via impregnation with metal oxides, clay minerals, organic compounds, or carbonaceous materials such as graphene oxide, polysaccharides, and carbon nanotubes to synthesize biochar composites (Ok et al., 2015). The addition of different components into biochar improves surface functionalities, which in turn, enhances the adsorption performance for a wide range of contaminants, though it may occasionally decrease the porosity in engineered biochar composites via blockage of pores (Tan et al., 2016b; Xiang et al., 2020). Biochar is known to provide support and host foreign particles within its porous matrix such as clay, trace metals and other inorganic nutrients. This property of biochar has been further exploited for the synthesis of engineered clay-biochar composite with enhanced value and functions in terms of their applications (Yao et al., 2014). The most recent research focus for the designer biochar is assembling Layered Double Hydroxides (LDHs) as a win-win approach for synthesizing mineral-biochar composites, as it improves adsorption performance owing to the enhanced particle stability, surface activity, functional group density, and recoverability (Yang et al., 2019). Moreover, LDHs tailored biochar composites show photocatalytic and sonocatalytic degradation potential of organic pollutants, in particular antibiotics (Gholami et al., 2020a; Gholami et al., 2020b).

Layered double hydroxides (LDHs) are known as hydrotalcite-type anionic clay, consisting of stacked positive layers, which are separated and neutralized by exchangeable anions in the interlamellar galleries (Yan et al., 2016). LDHs are assembled by a non-covalent bond, where the positively charged main lamellar includes divalent or trivalent cations and non-framework interlayer anions along with water molecules (Mishra et al., 2018). Intriguing properties of LDHs such as straightforward facile synthesis, uniformly distributed layered lamellar structure, presence of surface hydroxyl groups, easy tunability, intercalated anions with interlayer spaces, high chemical and thermal stability, high capability and compatibility to intercalate various inorganic, organic, biomolecules, and even genes (Daud et al., 2019; He et al., 2018) make them unique to be used in composite materials. Unique characteristics of LDHs make it useful in various applications such as the photocatalytic generation of H_2, CO_2 reduction, electrocatalytic evolution of O_2, as an electrode material and application in contaminants removal (Mohapatra and Parida, 2016; Zhao et al., 2017). Moreover, LDHs are alkaline and positively charged due to the nature of metal cations and metal—O bonds, which provision for electrostatic interactions with anionic pollutants, thus, covering the limitation of biochar (Huang et al., 2019). Conversely, a condensed multilayer stacked structure of standalone LDHs as adsorbent may limit the efficacy to uptake diverse pollutants (Jia et al., 2019). Therefore, assembling LDHs into biochar becomes a win-win strategy for both biochar and LDHs, in terms of adsorptive removal of numerous contaminants from water.

Many studies have been reported on LDHs—biochar composites in the literature that are used for the enhanced removal of diversified

contaminants viz., toxic metals, metalloids, dyes, nutrients, pharmaceuticals, and personal care products (dos Santos Lins et al., 2019; Wang et al., 2016; Zhang et al., 2018b). Properties of the composite may differ significantly from each other due to the feedstocks used, production conditions of biochar, composite material types, and synthesis technique of the LDHs. However, not much studies yet are available to understand the factors that influence the properties of LDHs-biochar composites. As the use of biochar alone may have some limitations on its use as an adsorbent, the biochar composites could be considered a better option to address the challenges. Hence, it is timely to summarize the LDHs tailored biochar assemblages in order to design the appropriate composite for the simultaneous removal of different contaminants efficiently and to understand the underlying mechanisms. Therefore, the objective of this mini-review is to (1) summarize the fabrication techniques of LDHs tailored biochar composites via different approaches; (2) discuss comprehensive characterization of the composites; (3) assess the adsorption performances through kinetics and isotherms data reported for various contaminants and (4) elucidate possible synergistic mechanisms in tailored LDHs-biochar assemblage as composite materials for contaminants removal from water.

2. Layered double hydroxide assembled biochar composites

Various divalent and trivalent cationic metals have been employed to tailor LDH biochar composites. Synthesis techniques are also varied from each other to influence the final objective of the composite application. Three different methods have been used for the synthesis of LDH-biochar composites; 1) pre-coating the feedstock with LDH and pyrolysis after precipitation, 2) direct application of biochar to the cation precursor mixture and LDH synthesis, and 3) LDH synthesis on biochar-cation precursor mixture and pyrolysis again (Fig. 1). However, only one individual study reports the use of the latter two tailoring methods to prepare composites, which allows the comparison of the techniques (Wang et al., 2016).

2.1. Synthesis of LDH

Liquid phase co-precipitation method for the synthesis of LDHs has been widely reported; however, in some cases, co-precipitation was used as pre-coating method on biomass, before pyrolysis (Huang et al., 2019; Meili et al., 2019). Foremost, the composition and structure of the LDHs are governed by the synthesis methods. Co-precipitation, hydrothermal synthesis, urea hydrolysis, sol-gel method, mechano-chemical milling are among the most common methods that are used for the synthesis of LDHs (Theiss et al., 2016). Co-precipitation is often described as a "one-pot" method due to its simplicity and cost-effectiveness (Bukhtiyarova, 2019).

2.1.1. Tailored composites

Co-precipitation processes that have been utilized for tailoring the LDH-biochar composite in the literature are mainly two; 1) addition of biochar to the cation precursor mixture before precipitation, and 2) pretreating the biomass with the precursor, synthesizing LDH followed by pyrolysis (dos Santos Lins et al., 2019; Jiang et al., 2019; Tan et al., 2016b; Wang et al., 2016). Among these, the addition of biochar to the cation precursor mixture and precipitation is the most common technique, used in composites preparation (Table 1). Since pre-coating and precipitation on the feedstock before pyrolysis may reduce the yield of the composite, experimental lab-scale studies have used higher amounts of feedstocks such as 3–25 g, in average 10 g, for the composites preparation, whereas the direct addition of biochar is used <2 g (Yu et al., 2018; Zhang et al., 2018b). Interestingly, aging and heating times, and heating conditions, used in the studies, vary profoundly. Most published works have reported 1–3 days for aging the precipitate (Bolbol et al., 2019; Cui et al., 2019; Li et al., 2016; Xue et al., 2016). Mg/Al and Mg/Fe as the leading LDHs have been reported
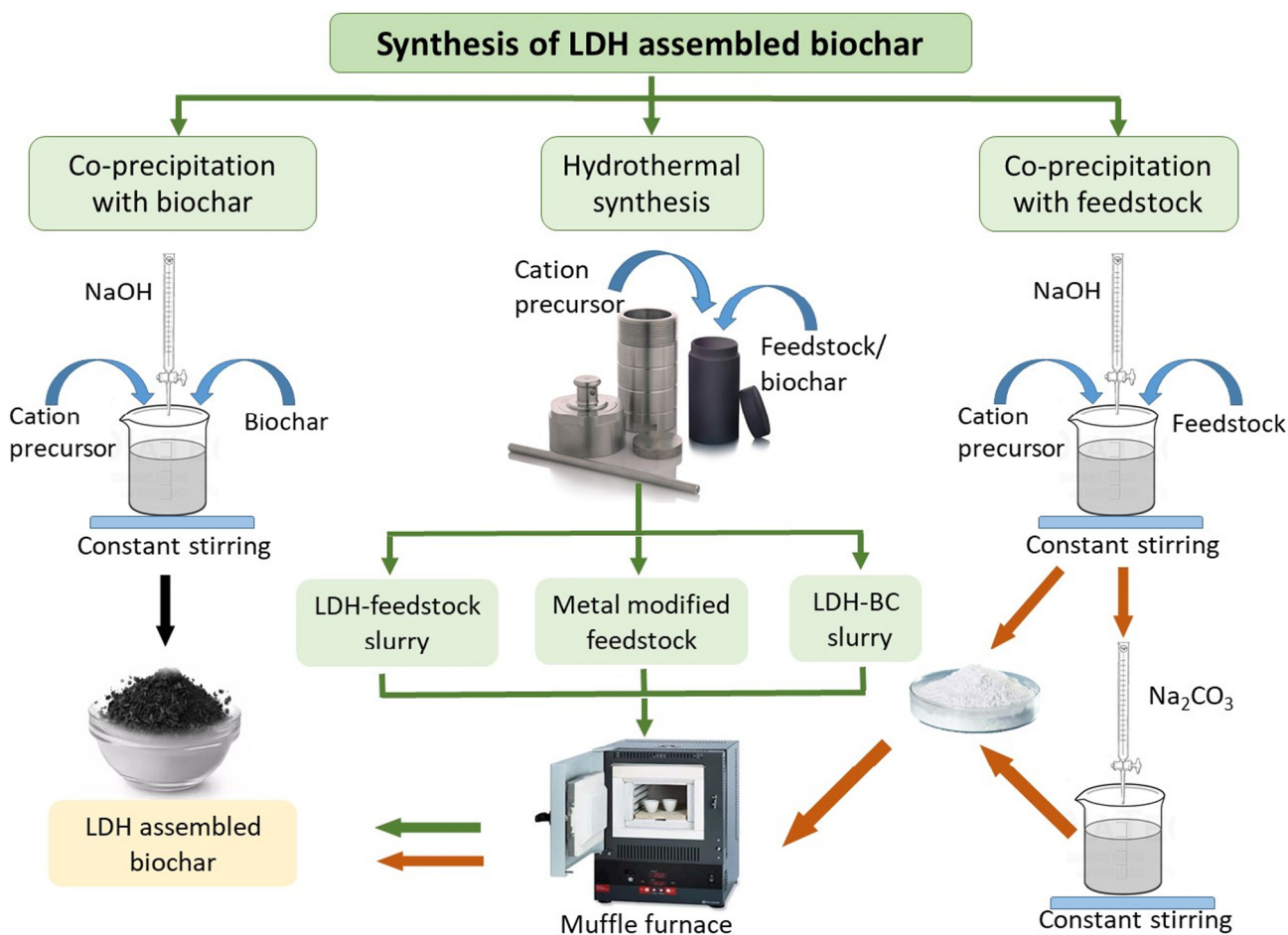
Fig. 1. Different techniques for the synthesis of LDH-biochar.

for biochar composite synthesis through co-precipitation. About 50% of the studies reported in the literature have used $AlCl_3 \cdot 6H_2O$ and $MgCl_2.6H_2O$ as the cationic precursors, whereas the ratios used are different, mostly in 1:3 ratio.

The other frequently used cation precursors are $MgCl_2.6H_2O$ and $FeCl_3.6H_2O$. $ZnCl_2$, $AlCl_3$, $Ni(NO_3)_2$, $FeCl_3 \cdot 6H_2O$, $Fe(NO_3)_3$ and $Mg(NO_3)_2$ have rarely been used to synthesize LDH-biochar assemblages (Table 1). In many studies (about 40%), biochars used for LDH tailored composite synthesis, have been pyrolyzed at 600 °C. Interestingly, only a few studies have utilized biochars, prepared at low and high temperatures, i.e., <450 °C and >700 °C, whereas the majority of the biochars were produced at an average temperature of 500 °C. Studies related with the comparison of different syntheses techniques, various feedstock types, pyrolyzed temperatures etc. may be helpful in order to understand the mechanisms to produce composites with improved properties.

A study applied co-precipitation of oil-tea camellia shells magnetic biochar in cation precursor followed by hydrothermal synthesis at 120 °C for 6 h in an autoclave reactor (Jia et al., 2019), while another study reported the hydrothermal synthesis of banana straw powder together with urea and cation precursor mixture at 110 °C for 4 h, before the pyrolysis at 500 °C for 4 h (Jiang et al., 2019). Hydrothermal synthesis of Al-modified biochar with $MgSO_4$ and urea, was reported in a recent study, where the Al-modification was done with soaking pinewood saw dust in $Al(NO_3)_3 \cdot 9H_2O$ and ethanol (Wang et al., 2020). A high surface area, 405 m^2/g was reported from this process which is suitable as an adsorbent. It is evident that various types of fusion techniques may result in diverse characteristics, which are unable to compare, signifying the importance of studies to compare the

properties based on the synthesis conditions. Among other synthesis methods, an electro-tailored method was used to prepare *Caragana korshinskii* biochar/Mg–Al LDH composite with a current density of 124 mA/cm^2) for 5 min (Cui et al., 2019). It is evident from the literature that although various techniques have been used for synthesizing LDH assembled biochar composites, in-depth molecular level studies are deficient to conclude which methods suit the particular purpose.

2.2. Characterization of LDH-biochar composites

Layered double hydroxide tailored biochar composites have been well characterized by employing spectroscopic techniques such as X-Ray diffraction and Fourier Transform Infrared spectroscopy mainly for their structure and composition, and specific surface area analysis by Brunauer–Emmett–Teller (BET) method. X-Ray photoelectron spectroscopy (XPS) and Thermo-Gravimetric analysis (TGA) data have been reported by few studies, whereas some other studies have reported the elemental composition specifically, C, H, N and metal ions (Jiang et al., 2019; Yang et al., 2019). A study reported the particle size of the co-pyrolyzed composite as mainly in between 40 and 60 μm in size (Lee et al., 2019), whereas another composite ranged 50–300 nm with a saturation magnetization of biochar was 21.57 emu/g (Jia et al., 2019). A similar saturation magnetization value was reported for magnetic *Caragana korshinskii* biochar/Mg–Al LDH composite as 33 emu/g (Cui et al., 2019).

2.2.1. Physical properties of LDH assembled biochar composites
The most common physical properties related to the characterization studies reported for LDH-biochar composites are surface area,

Table 1
Layered Double Hydroxide tailored biochar synthesis techniques under different conditions.

Composite type	Biochar condition	LDH type	Preparation method	Cation precursors	Molar ratio	Feedstock/Biochar amount	Time of feedstock/biochar addition	Remarks	Reference
MgAl-LDH/biochar composite	NA	Mg/Al	Co-precipitation	$AlCl_3 \cdot 6H_2O$ & $MgCl_2.6H_2O$	1:2	1 g	To the cation precursor mixture	4 h settling time	(dos Santos Lins et al., 2019)
Biochar/MgAl-LDH ultra-fine composites	600 °C under N_2	Mg/Al	Spontaneous self-assembly method	$MgCl_2.6H_2O$ & $AlCl_3.6H_2O$	3:1	10 g	To the cation precursor mixture	Aged for 3 d at 80 °C before washing	(Zhang et al., 2013)
Ni/Fe LDH-biochar composites	600 °C under N_2	Ni/Fe	Co-precipitation	$Ni(NO_3)_2$ & $FeCl_3.6H_2O$	1:1	25 g	Co-precipitation on the feedstock	Feedstock soaked in precursor solution before precipitation	(Wang et al., 2016)
					2:1	5 g	To the cation precursor mixture	No aging	
LDH loaded biochar	300 °C under Ar	Mg/Fe	Co-precipitation	$MgCl_2.6H_2O$ & $FeCl_3.6H_2O$	3:1	10 g	To the cation precursor mixture	Aged for 1 d at 70 °C before washing	(Bolbol et al., 2019)
Magnetic biochar/MgFe-LDH	600 °C under N_2	Mg/Fe	Hydrothermal synthesis	$Fe(NO_3)_3$ & $Mg(NO_3)_2$	1:2	2 g	To the cation precursor mixture	Aged at 120 °C for 6h	(Jia et al., 2019)
Carbon supported calcined-Mg/Al LDH	475 °C	Mg/Al	Modified liquid-phase deposition	$MgCl_2.6H_2O$ and $AlCl_3.6H_2O$	3:1	20 g	Precipitate on to the precoated feedstock	Feedstock & cation precursor slurry was aged at 100 °C for 1 d	(Tan et al., 2016c)
Biochar assembled LDH	600 °C under N_2	Zn/Al Mg/Al Ni/Fe	Co-precipitation	$ZnCl_2$ and $AlCl_3$ $MgCl_2.6H_2O$ and $AlCl_3.6H_2O$ $Ni(NO_3)_2$ and $FeCl_3 \cdot 6H_2O$	2:1	3 g	Precipitate on to the precoated feedstock		(Yang et al., 2019)
Mg-Fe LDH-Kiwi branch biochar	500 °C under N_2	Mg/Fe	Liquid phase deposition	$MgCl_2.6H_2O$ and $FeCl_3.6H_2O$	3:1	10 g	To the cation precursor mixture	Aged for 3 d at 80 °C before washing	(Tan et al., 2019)
MgAl-LDH pre-coated ramie biomass	500 °C	Mg/Al	Co-precipitation	$AlCl_3 \cdot 6H_2O$ and $MgCl_2.6H_2O$	1:3	20 g	Precipitate on to the precoated feedstock	Precipitated slurry was aged at 100 °C for 1 d	(Tan et al., 2016a)
Biochar with Mg—Al and Mg—Fe LDH	600 °C under N_2	Mg/Al Mg/Fe	Spontaneous self-assembly method	$MgCl_2.6H_2O$ and $FeCl_3.6H_2O$ $MgCl_2.6H_2O$ and $AlCl_3.6H_2O$	3:1	10 g	To the cation precursor mixture before dropwise addition of NaOH	Aged for 3 d at 80 °C before washing	(Wan et al., 2017)
Rice husk ash Mg—Fe LDH	NA	Mg/Fe	Co-precipitation	$Mg(NO_3)$ $2.6H_2O$, Fe $(NO_3)_3.9H_2O$	3:1	0.2 g	To the cation precursor before NaOH addition	Feedstock and cation precursor slurry was aged for 24 h	(Yu et al., 2018)
Mg-Al LDH functionalized biochar	550 °C under N_2	Mg/Al	Co-precipitation	$Mg(NO_3)_2$ and $Al(NO_3)_3$	3:2	10 g	To the cation precursor before NaOH addition	Aged for 3 d at 80 °C before washing	(Li et al., 2016)
Polyporous LDH biochar composite	600 °C under N_2	Mg/Fe	Co-precipitation	$MgCl_2.6H_2O$ and $FeCl_3.6H_2O$	5:1	20 g	To the cation precursor before KOH addition	Feedstock was pretreated and aged for 1 d at 70 °C	(Zhang et al., 2018b)
Biochar-MgAl LDH nanocomposite	700 °C	Mg/Al	Co-precipitation	$MgCl_2.6H_2O$ and $AlCl_3.6H_2O$	3:1	10 g	To the cation precursor before NaOH addition	Aged for 1 d at 90 °C before washing	(Alagha et al., 2020)
Biochar modified LDH	700 °C	Mg/Al	Co-precipitation	$MgCl_2.6H_2O$ and $AlCl_3.6H_2O$	3:1		To the cation precursor before NaOH addition		(Huang et al., 2019)
Syagrus coronata biochar-MgAl LDH	400 °C	Mg/Al	Co-precipitation	$MgCl_2.6H_2O$ and $AlCl_3.6H_2O$	2:1	1 g	To the cation precursor before NaOH addition		(de Souza dos Santos et al., 2020)
Magnetic *Caragana korshinskii* biochar/Mg-Al LDH	600 °C under N_2	Mg/Al	Electrochemical method	$MgCl_2$ electrolyte and aluminuim electrode		3 g	A current density was applied for 5 min using a power supply and aluminum electrodes	Aged for 1 d at 80 °C and oven-dried at 60 °C under a N2 environment	(Cui et al., 2019)
Biochar/MnAl-LDH	600 °C	Mn/Al	Hydrothermal synthesis	$MnSO_4$, Al $(NO_3)_3$	2:1	1 g	To the cation precursor before Na2CO3 and NaOH addition	After NaOH addition Teflon-lined stainless-steel autoclave at 100 °C for 1 h	(Wang et al., 2018)
MgFe-LDH modified wheat straw biochar	600 °C under N_2	Mg/Fe	Co-precipitation	$MgCl_2.6H_2O$ and $FeCl_3.6H_2O$	3:1	10 g	To the cation precursor before NaOH addition	Aged for 3 d at 70 °C before washing	(Xue et al., 2016)
Mg/Al-calcined	500 °C	Mg/Al	Co-precipitation	$Mg(NO_3)_2$		1 g	Precipitated on to the	Aged for 3 d at 50 °C before	(Lee

Table 1 (continued)

Composite type	Biochar condition	LDH type	Preparation method	Cation precursors	Molar ratio	Feedstock/Biochar amount	Time of feedstock/biochar addition	Remarks	Reference
LDH-rice husk biochar				and $Al(NO_3)_3$			feedstock	washing	et al., 2019)
Vegetable biochar-LDH Rape	500 °C	Mg/Al	Co-precipitation	$Mg(NO_3)_2$ & $Al(NO_3)_3$	2:1	10 g	Precipitated on to the feedstock	Feedstock and cation precursor mixture was stirred for 12 h and statically crystallized for 6 h at 60 °C	(Zhang et al., 2019)
MgAl-LDH/Biochar	600 °C under N_2	Mg/Al	Co-precipitation	$MgCl_2.6H_2O$ & $AlCl_3.6H_2O$	2:1	1 g	To the cation precursor before NaOH addition		(Meili et al., 2019)
Banana straw ZnAl-LDH	500 °C	Zn/Al	Hydrothermal synthesis	$ZnCl_2$ & $AlCl_3$	5:1	1 g	Mixed with cation precursor and hydrothermally synthesized	Cation precursor mixture was subjected to 110 °C for 4 h	(Jiang et al., 2019)
Pine wood saw dust	350 °C	Mg/Al	Hydrothermal synthesis	$Al(NO_3)_3 \cdot 9H_2O$ & $MgSO_4 \cdot 7H_2O$	3:1	5 g	Al soaked feedstock was pyrolyzed and hydrothermally synthesized with urea & Mg salt	Autoclaved for 160 °C for 10 h	(Wang et al., 2020)

pore-volume, pore diameter, structural and, thermal characteristics (Table S1).

2.2.1.1. Surface area. In general, biochar with high surface area has been subjected to the composite formation with different types of LDHs. The resulting composites have shown a less specific surface area, low pore-volume, and small pore diameter due to the deposition of LDH into biochar's pore structure. Kiwi branch biochar was used as the raw material for composite preparation which originally had a specific surface area of 31 m²/g, however surface area was reduced by 20 times to 1.5 m²/g in the composite (Tan et al., 2019). In this study, the precipitation of the LDH was done in the biochar mixture, which may lead to reduction in BET surface area. Pristine biochar with a BET surface area of 182 m²/g decreased to 4 m²/g, suggesting pore filling via impregnation on biochar surfaces (Xue et al., 2016). Similarly, composite synthesized by pre-coating the feedstock by LDH precipitation, reported low surface area as 9.8 m²/g (Tan et al., 2016a). However, in some cases, the BET surface area of the composite has shown an increase than that of the biochar, which may be due to the higher surface area of the pristine LDH. A recent study reported a high surface area of composite (>160 m²/g) than the plant-derived biochar (71 m²/g), though the pore volume was decreased considerably, indicating impregnation of biochar with the LDH (de Souza dos Santos et al., 2020). An interesting study compared composites, synthesized in two different techniques; biochar was used directly in LDH precipitation, and post-pyrolyzed LDH-biochar composite. The results demonstrated that the post-pyrolysis increased the surface area than that of the pristine biochar and LDH (Wang et al., 2016). Impregnated LDH in biochar clearly showed a substantial reduction of BET surface area as expected from 335 m²/g of pristine biochar to 174 m²/g of composite. Some studies reported high values of the surface area as: 201, 246, 405 and 441 m²/g for rice husk powder, ash and date palm as the feedstock, despite different synthesis conditions (Alagha et al., 2020; Lee et al., 2019; Wang et al., 2020; Yu et al., 2018). Rice husk ash and date palm biochar were directly used for co-precipitation (Alagha et al., 2020; Yu et al., 2018), whereas rice husk powder was pre-loaded with cation precursor followed by co-pyrolysis (Lee et al., 2019). The study reported the surface area data for different co-pyrolysis temperatures demonstrating an increase from 52 to 246 m²/g for the temperatures from 300 to 500 °C, respectively, due to calcination, and a decline to 104 at 700 °C (Lee et al., 2019). However, no explanations were given for the decrease in surface area at high temperatures, which may be owing to the formation of ash, which is accountable to >67% *w*/w (Yu et al., 2018). Hydrothermally synthesized novel magnetic LDH-biochar composite showed >2 times higher BET surface area (86 m²/g) than that of the pristine magnetic

biochar (37 m²/g), which was evidenced due to LDH incorporation in some cases (Jia et al., 2019). A recent hydrothermal synthesis of Mg/Al LDH assembled pine wood biochar composite demonstrated high surface area compared to most other studies (Table S1), however, BET surface area of the composite (405 m²/g) was less than that of the pristine biochar, which was 539 m²/g (Wang et al., 2020). In-depth studies are essential to understand the influence of composite synthesis method, biochar feedstock, or temperature on the specific surface area, as a clear relationship is not visible in most studies.

2.2.1.2. Pore volume and pore diameter. A few studies have reported the pore volume and pore diameter data though no relationship can be observed due to the limited information presented in the literature. Pore diameter ranged from 3 to 22 nm, whereas the highest pore volume was reported as 1 cm³/g in a study, where authors used rice husk ash biochar (Yu et al., 2018). Furthermore, it was observed that the pore volume of the pristine rice husk ash and LDH was less than that of the composite, although it was contrary to the pore diameter data. The only study which reported data from composites, co-pyrolyzed at different temperatures from 300 to 700 °C, demonstrated an increment of pore volume and pore diameter with the increase in temperature and a decline after 500 °C (Lee et al., 2019). A significant improvement of pore volume from 0.4 to 0.8 cm³/g, was observed in hydrothermal synthesis of Al-modified pine wood biochar with urea and Mg salt indicating the formation of mesoporous structure during hydrothermal process (Wang et al., 2020). Corroborated data were observed from a novel magnetic biochar-LDH composite where the pore volume was three times higher in the composite (0.045 cm³/g in biochar and 0.13 cm³/g in composite), though the pore diameter data was three times lower (20 nm) than that of the pristine magnetic biochar (7 nm in composite) (Jia et al., 2019).

2.2.1.3. Yield and proximate analysis. Data related to the yield of LDH-biochar composite lacks in literature. Only one study reports the yield for the biochar, MgAl/LDH and MgAl/LDH-biochar composite where yields were reported as 38.9, 68.7 and 71.8%, respectively, calculated through the mass balances (de Souza dos Santos et al., 2020). Yield is governed not solely by the synthesis process, but also the operation process, mainly washing of the material is a crucial factor, besides the biochar production temperature and the feedstock. However, biochar production conditions and feedstock matter only, if the pyrolysis is done after the precipitation.

2.2.1.4. Structural and thermal characteristics. Powder X-Ray Diffraction (PXRD) and Thermo Gravimetric Analysis (TGA) data reveal the

structural and thermal characteristics of biochar/LDH composites. A comparison between the XRD patterns of parent biochar and biochar-LDH composite clearly confirms the formation of LDH on biochar surface together with few mineral peaks in biochar (Wang et al., 2020). Based on feedstock materials, some biochar types have demonstrated quartz peaks due to the presence of Si (Tan et al., 2019; Xue et al., 2016). Zhang et al. (2013) have confirmed the formation of ultra-fine composite of biochar-Mg/Al-LDH with the XRD pattern of pure hydrotalcite (Zhang et al., 2013), which is a characteristic mineral peak of LDH (Bolbol et al., 2019). The unit cell parameters and interlayer space of LDH can be calculated using the XRD spectrum data. LDH interlayer space can facilitate the adsorbate ions or molecules to be trapped in-between with new bonds between LDH layer and itself. The successful co-precipitation of LDH on biochar is confirmed by the crystallographic parameters (Bolbol et al., 2019). Corresponding crystal planes are recognized with the peaks at appropriate 2θ values. Jia et al. (2019) reported characteristic peak for cellulose crystal plane at around 24.1° and apparent peaks confirmed the presence of Fe_3O_4 crystalline phases and $Mg_6Fe_2CO_3 (OH)_{16}•4H_2O$ diffraction peak for biochar-Mg/Fe-LDH composite (Jia et al., 2019).

Furthermore, scanning electron microscope (SEM) images revealed surface morphological data of the composite. SEM images confirmed the homogeneous deposition of Mg/Al-LDH flakes with sharp edges and corners on the biochar surfaces (Li et al., 2016). Similarly, SEM-EDS analysis results exhibited elemental impurities and their distribution in the biochar/clay-composite, depending on the feedstock material of biochar and LDH minerals, such as Mg, Al, Fe and Ni (Wang et al., 2016; Zhang et al., 2013). The smooth surface of pristine biochar and the rough surface with homogenously covered LDH nano-sized particles were observed from SEM images (Bolbol et al., 2019). However, Transmission electron microscopy (TEM) confirmed the collapse of the layered structure of LDH and calcination, resulting in Mg and Al oxides (Tan et al., 2016c). The hexagonal dimensions of the layered structure were invisible after calcination (Fig. S1). Zhang et al. (2018) have reported a peak in XRD spectrum for brucite, which is the mineral form of magnesium hydroxide (Zhang et al., 2018b).

The thermal stability of the LDH assembled biochar composites was evaluated with thermogravimetric analysis (TGA). Mass loss of the composite has been analyzed in a range of temperature with a heating rate under N_2 atmosphere (Yang et al., 2019). The first significant mass loss in the graph demonstrates the removal of adsorbed water molecules on composite surface and the second mass loss exhibits the decomposition of the components of the composite such as transformation of metal hydroxides to oxides (Meili et al., 2019). The final weight percentages of the composites clearly indicate the relative thermal stability of the composites. Decomposition, which is a chemical reaction, transitions, and oxidation, decrease the composite mass (de Souza dos Santos et al., 2020). Therefore, temperature bands can be observed by plotting the mass % versus temperature.Chemical properties of LDH assembled biochar composites.

2.2.2. Surface functional groups

Surface functional groups of ultra-fine biochar/LDH composites were analyzed using FTIR spectra (Table S2). A comparison of pristine biochar and biochar/LDH composites confirms the formation of the composite, through newly generated FTIR bands (Jia et al., 2019). Based on the biochar type and the metals/chemicals used in LDH, the new bands can vary. Owing to the presence of a large number of hydroxyl groups, interlayer, and physically absorbed water, the absorption bands of -OH stretching and vibration were observed around 3400 and 1630–1640 cm^{-1} (Zhang et al., 2013). The low-frequency vibrational bands present in 400–1000 cm^{-1} have represented metal-oxygen bonds; M—O and O—M—O, which implies in the translational motion of the oxygen-cation in LDH layers (Bolbol et al., 2019; Tan et al., 2016c). Some LDHs, which contain Na_2CO_3 as a precursor material, exhibited stretching vibrational band around 1380 cm^{-1} corresponding

to interlayer CO_3^{2-}. Similarly, the vibrational band for CO_3^{2-} has a possibility to appear as a result of CO_2 in the air (Tan et al., 2016c; Yang et al., 2019). However, Santos et al. reported a band around 1360 cm^{-1}, which is due to CO_3^{2-} in MgAl/LDH supported on *Syagrus coronata* biochar composite (de Souza dos Santos et al., 2020). Furthermore, FTIR bands of both asymmetric and symmetric vibrations of CO_3^{2-} were present in biochar/MnAl-LDH composite. Few studies have reported NO_3^- bands in the range of 1360–1370 cm^{-1} (Alagha et al., 2020; Yu et al., 2018).

The asymmetric stretch of long-chain aliphatic components from biochar structure has determined a band around 2900 cm^{-1} (Bolbol et al., 2019). The other functional groups of biochar, such as C==O stretching vibration, and alcoholic C—OH exhibited bands around 1630 and 1030 cm^{-1} (Bolbol et al., 2019; Tan et al., 2016c). Furthermore, C—O of CO_3^{2-} was assigned to 1413 and 1374 cm^{-1} proving interlayer anions (Wang et al., 2020). Band wavelengths for aromatic C==C varies with the preparation method of the composite. Calcined biochar/LDH composites have demonstrated aromatic C==C bands around 1630 cm^{-1}, while non-calcined composites showed bands around 1450 cm^{-1} (Bolbol et al., 2019; Tan et al., 2016c). Bending vibrations of aliphatic –CH_2 and –CH_3 groups presented at the band values of 1440 and 1380 cm^{-1} (Tan et al., 2016c). Based on the biochar/LDH composites, FTIR bands for numerous functional groups such as C—O—C, P—O, aliphatic C—O—O, asymmetric, and aromatic C—H can be observed (Li et al., 2016). The intensities of the bands are directly proportional to the number of functional groups on the biochar surface (Tan et al., 2016a). Amino and NO_3^- are some of the specific functional groups that are unique for a particular biochar/LDH composite (Yu et al., 2018). The bands around 1645 cm^{-1} revealed amino groups, while NO_3^- groups in interlayer space have confirmed by bands around 1365 cm^{-1}. Symmetric vibrations of Si—O—Si were reported around 1000–1100 cm^{-1} (Zhang et al., 2018b).

3. Adsorptive removal of contaminants from water by LDH tailored biochar composites

LDH-biochar composites have recently been studied for environmental remediation, despite the fact that the research in the past has been conducted for LDH and biochar separately. However, interestingly, LDH assembled biochar composites have been examined for many different types of environmental contaminants such as potentially toxic elements, i.e. As(V), Pb(II), Cr(VI); inorganic nutrients, i.e. phosphate and nitrate; dyes, and pharmaceuticals (Table 2).

3.1. Potentially toxic elements

A number of potentially toxic elements (PTEs) have been studied for their removal from water by biochars, decorated by various types of LDHs. Among different PTEs, anionic metals, metalloids, and cationic metals have been studied for their successful removal, though studies on As(V) and Cr(VI) are limited (Huang et al., 2019; Wang et al., 2016). As(V) removal by Ni/Fe LDH-pine wood biochar composite was found to be higher, however, showed similar removal kinetics for both post and pre-pyrolyzed composites (Wang et al., 2016).

Contrary to kinetics, pH edge data indicated two times higher removal of As(V) (from 1.4 to 4.3 g/kg) by the post-pyrolyzed LDH-biochar composite, specifically at low pHs, i.e. pH 3. Similarly, post-pyrolyzed composite exhibited two times higher (1.5 to 4.4 g/kg) adsorption capacity for As(V) in isotherm experiments (Wang et al., 2016). Maximum adsorption capacity of the composite was >2.5 times higher than that of the pristine pine wood biochar for As removal (Wang et al., 2016). The adsorption of Cr(VI) has also been investigated with a maximum removal capacity in the range of 36–38 mg/g (Huang et al., 2019; Wang et al., 2020). Adsorption of Cr(VI) was highly favorable in the acidic pHs due to the speciation of the metal and surface charge of the composite, which is positive in acidic pHs (Huang et al., 2019). Highest adsorption capacity (330 mg/g) was reported for the

Table 2
Layered double hydroxide tailored biochar composite used in adsorptive removal of different contaminants, experimental conditions, capacities and performances.

Biochar type	Temperature	LDH type	Contaminants removed	Experimental conditions			Adsorption Capacity mg/g		Performance (partition coefficient) L/g	Removal rate g/mg min	Reference
				Adsorbent dose, g/L	Initial concentration for kinetics, mg/L	Concentration range for isotherm, mg/L	Raw BC	Composite			
Bovine bone activated biochar	NA	Mg/Al	Caffeine	4	15	0–200		26	0.17	0.37	(dos Santos Lins et al., 2019)
Cotton wood	600 °C under N_2	Mg/Al	Phosphate	0.1	50	10–800		410	0.2×10^{-3}	0.70	(Zhang et al., 2013)
Pine wood	600 °C under N_2	Ni/Fe	As(V)	2.5	20	0–40	1.6	4.4	0.1×10^{-3}	0.17*	(Wang et al., 2016)
Pine cone flakes	300 °C under Ar	Mg/Fe	Phosphorous	5	100	5–300	1.4	17.5	0.08	0.02	(Bolbol et al., 2019)
Magnetized oil-tea camellia shells	600 °C under N_2	Mg/Fe	Pb	0.4	50, 100 and 200	10–480		476	1.48	0.011, 0.013 and 0.017	(Jia et al., 2019)
Bagasse	475 °C	Mg/Al	Tetracycline	1	20	20–500		1118	–	0.004	(Tan et al., 2016c)
Corn stalk powder	600 °C under N_2	Zn/Al Mg/Al Ni/Fe	Phosphate	0.2	50	10–200		152 65 78	– – –	0.25 0.05 0.02	(Yang et al., 2019)
Kiwi branch	500 °C under N_2	Mg/Fe	Cd	0.4	50	0.5–100	1.8	25.6	0.32	0.04	(Tan et al., 2019)
Ramie biomass	500 °C	Mg/Al	Crystal violet	1	500	50–500		374	2.68	8.988×10^{-4}	(Tan et al., 2016a)
Bamboo	600 °C under N_2	Mg/Al	Phosphate	2	10 and 50	5–600		172	0.11 –	6.7 and 2.1*	(Wan et al., 2017)
Rice husk ash	NA	Mg/Fe	Pb Cu Co Ni Zn Cd	0.5	10			100 54 7 34 29 29	1.1×10^3 19.4 0.87 5.13 4.39 4.1	0.12 0.07 0.34	(Yu et al., 2018)
Sugar cane harvest trash	550 °C under N_2	Mg/Al	Phosphate	2.5	50	5–500		82	0.27	0.78	(Li et al., 2016)
Rice straw	600 °C under N_2	Mg/Fe	NH_4 NO_3 Cu Zn Ni Pb Cd	3.3 3.3	500 1000			98 27 296 142 76 1264 126	0.02 0.03 0.64 0.4 0.4 0.75 1.85		(Zhang et al., 2018b)
Date palm	700 °C	Mg/Al	Nitrate Phosphate			10–50		28 178	0.64 6.02	1.96×10^{-5} 4.88×10^{-5}	(Alagha et al., 2020)
Bamboo shavings	700 °C	Mg/Al	Cr(VI)	1	50	20–250		38	0.25	3.0×10^{-4}*	(Huang et al., 2019)
Ouricuri (Syagrus coronata)	400 °C	Mg/Al	Diclofenac	4	30	50–200		139	0.43		(de Souza dos Santos et al., 2020)
Magnetic Caragana korshinskii biochar	600 °C under N_2	Mg/Al	Phosphate	1	50	5–500		253	0.74	0.16	(Cui et al., 2019)
Oil-tea camellia shells	600 °C	Mn/Al	Cu	3.2	100	40–350		74	0.6	0.008	(Wang et al., 2018)
Wheat-straw	600 °C under N_2	Mg/Fe	Nitrate	2	50	0–88		25	0.16	0.11	(Xue et al., 2016)
Rice husk	500 °C	Mg/Al	Phosphate	1.25	25, 50 and 100	5–500		149	1.68	0.04, 0.02 and 0.03	(Lee et al., 2019)
Chinese cabbage Rape	500 °C	Mg/Al	Phosphate	2.5	50	0–200		127 132	0.63 0.67	0.05 0.28	(Zhang et al., 2019)
Bovine bone biochar	600 °C under N_2	Mg/Al	Methylene blue	2	100	5–500		406	1.44	0.036	(Meili et al., 2019)
Banana straw	500 °C	Zn/Al	Phosphate	4	300	5–600		185	1.73	0.05	(Jiang et al., 2019)
Pine wood saw dust	350 °C	Mg/Al	Pb Cr(VI)	0.2–1.0	50	10–500 10–300		591 330	1.18 1.10	5.3×10^{-4} 4.8×10^{-4}	(Wang et al., 2020)

Note: * is for kg/mg h.

hydrothermally synthesized Mg/Al pine wood biochar composite for Cr (VI) indicating chemisorption as the mechanism (Wang et al., 2020). Kinetics and isotherm experiments demonstrated a significant enhancement of Cr(VI) removal by the LDH decorated biochar composite compared to pristine biochar. The maximum adsorption capacity was found to be 55 mg/g for the LDH-bamboo biochar composite, whereas it was 27 mg/g in case of the pristine biochar (Huang et al., 2019). The presence of other ions demonstrated that the influence of Cl^- and NO_3^- ions was lower on Cr(VI) adsorption than that of $Cr_2O_7^{2-}$, however, SO_4^{2-} ions had a great influence for Cr(VI) removal. A recent study demonstrated least interference of NO_3^-, which may be attributed to the lower negatively charge density compared with Cr(VI), however, co-existing SeO_4^{2-} decreased the capacity from 105 to 80 mg/g, which may be due to the similarity of the structure and charge density (Wang et al., 2020). This indicates the need of similar studies in order to understand the practical applications of LDH/biochar composite to treat real wastewater containing other anions.

A large number of studies have reported the removal of cationic PTEs, e.g. Pb(II), Cd(II) etc. by LDH tailored biochar composites. Pristine Kiwi branch biochar demonstrated 1.8 mg/g adsorption capacity for Cd (II), whereas a significantly higher adsorption capacity was reached by its LDH composite with 25.6 mg/g (Tan et al., 2019). Hydrothermally synthesized magnetized oil-tea camellia shell biochar-LDH composite was examined for Pb(II) adsorption and an adsorption capacity was reported as 476 mg/g, which is seven times greater than that of the pristine magnetic biochar, suggesting a strong chemisorptive removal (Jia et al., 2019). The corresponding partition coefficient was 1.5 L/g, comparatively high compared to other performance data (Table 2). Favorable removal was observed in pH 3 to 6 with an increase of Gibbs free energy with increasing temperature, implying better adsorption at high temperature and positive enthalpy change indicating the interaction through endothermic reaction. A similar pH dependency was observed for Pb(II) adsorption with no ionic strength dependency indicating inner-sphere complexation of Pb(II) to the composite surface sites (Yu et al., 2018). Higher maximum adsorption capacity (682 mg/g) was reported for rice husk ash-LDH composite than that of the pristine LDH (317 mg/g) for Pb(II) removal with the best fit to Sips equation, which indicates the involvement of both monolayer and multilayer adsorption (Yu et al., 2018). Exceptionally high removal of Pb(II) was reported with 1264 mg/g Langmuir maximum adsorption capacity for rice straw biochar-LDH composite without showing any influence of media pH (Zhang et al., 2018b). Furthermore, relatively strong immobilization for Cu(II) and Pb(II) in sandy soil, compared to that of Zn(II), Ni (II), and Cd(II) by the addition of Mg/Fe-LDH@biochar was observed in simulated rainfall column experiments. Followed by the simulated rainfall, the majority of Pb(II) bound to the soil was around 15–35 cm depth (Zhang et al., 2018b).

A limited number of studies have focused their attention on co-existing ions for adsorption (Tan et al., 2019; Yu et al., 2018). Among the co-existence of electrolytes, NH_4Cl and $CaCl_2$ showed an influence on Cd(II) removal, whereas the effect from NaCl, KCl, and $NaNO_3$ was negligible due to the ion-sieve effect produced by the spatial limits between the brucite layers (Tan et al., 2019). For Pb(II), the presence of Ca and Na showed almost 5 times reduction from 261 mg/g, while the capacity slightly decreased to 228.0 mg/g with Na^+ respectively (Wang et al., 2020). The decrease of adsorption capacity was attributed to the competitive effect between heavy metal cations on the active sites. Cu(II) adsorption data corroborates with both Cd(II) and Pb(II) removal from LDH tailored biochar composites due to the valence similarities among these ions. About seven times higher maximum adsorption capacity (75 mg/g) for Cu(II) was observed for the hydrothermally synthesized composite of Oil-tea Camellia Shells biochar and Mn/Al LDH (Wang et al., 2018). In the case of Cu(II), the effect of coexistence cations such as Zn^{2+}, Ni^{2+}, Ca^{2+}, and Mn^{2+} exhibited no effect on Cu(II) adsorption, however, the adsorptions of Zn^{2+}, Ni^{2+}, Ca^{2+} and Mn^{2+} on the composite was lower compared Cu(II). Literature reports various coexisting ions in assessing the influence for adsorption, which limit the comparison between studies (Tan et al., 2019; Wang et al., 2018).

3.2. Inorganic nutrients

Among the inorganic nutrients, phosphate has been studied thoroughly by various LDH assembled biochar composites with successful removal capacities of >100 mg/g (Cui et al., 2019; Lee et al., 2019; Wan et al., 2017; Zhang et al., 2013). Comparative study on phosphate adsorption between the cottonwood biochar and its LDH composite indicated that the ultrafine uncalcined composite had a faster adsorption rate (1 h), which was similar to calcined composite, than pristine biochar (24 h) with an extremely high adsorption capacity of >400 mg/g (Zhang et al., 2013). Solution pH greatly influenced the phosphate removal, and in the case of LDH-magnetized biochar composite with variable charge surfaces, phosphate adsorption was prominent in acidic pHs via electrostatic attraction (Cui et al., 2019). The presence of Cl^-, NO_3^-, and SO_4^{2-} showed a negligible influence, whereas F^- competed and reduced the removal of phosphate in aqueous media. Bamboo biochar functionalized Mg—Al, and Mg—Fe (3:1) LDH, tested for phosphate adsorption, revealed that the phosphate-adsorbed composite has the potential to be used as a slow-release fertilizer with a successful lettuce seedling bioassay (Wan et al., 2017). Nitrate and phosphate removal using LDH tailored date palm biochar composite was found to be 28 and 178 mg/g respectively. Over 97% phosphate removal through strong adsorption and intercalation was observed by rice husk biochar decorated LDH due to the decomposition of interlayer water molecules, the transformation of LDH structures, and porosity (Lee et al., 2019). A significantly high performance has shown by the composite with 15 times higher adsorption for phosphate compared to its pristine pine cone biochar (Bolbol et al., 2019).

3.3. Dyes

Dyes in textile, dyeing, food, and paper industries have increasingly been utilized, and a large volume of poorly-treated or untreated dye wastewater poses the significant threats to the environment (Aksu et al., 2008; Sun et al., 2013). Different studies have been carried out where biochar and LDH could individually contributed for the adsorption of dyes; mostly cationic dyes and composite of the two were also tested for remediation of dyes (El Gaini et al., 2009; Meili et al., 2019; Tan et al., 2016a; Xu et al., 2011). Crop residue biochar assembled with calcined Mg-Al-LDH was used in methyl (crystal) violet removal which indicated reconstructing property of calcined LDH and interaction with the surface functional groups of biochar. The composite contributed to the high performance with an optimum adsorption capacity of 374 mg/g (Tan et al., 2016a). Furthermore, the removal of methylene blue from aqueous media by Mg-Al-LDH biochar composite, derived from Bovine bone (bone-char), synthesized by the co-precipitation method was studied by Meili et al. (2019. The adsorption capacity of 406.47 mg/g was obtained with comparatively high performance of 1.5 L/g compared to the partition coefficient values in Table 2. Weaker interactions were observed in the thermodynamic study, indicating mechanically resistant for re-utilization and regeneration of the adsorbent (Takehira, 2017; Tan et al., 2016a). Overall, the studies for dye removal using LDH assembled biochar composites are limited in literature.

3.4. Pharmaceuticals

Pharmaceutical compounds and residues are very often detected in water bodies. Biochar has shown promising removal performances over other natural materials e.g., clays for pharmaceuticals removal through π-π electron donor-acceptor interactions, hydrophobic interactions, van der Waal's forces and hydrogen bonding as predominant interactions (Ashiq et al., 2019; Premarathna et al., 2019a). *Syagrus*

coronate, an abundant plant in Brazil, was used for biochar production at 400 °C with Mg—Al cation precursor and was examined for its potential for diclofenac removal (de Souza dos Santos et al., 2020). Adsorption removal of 82% was achieved with the composite at environmental-relevant pH and the main mechanism for removal was suggested as electrostatic interaction. Mg-Al-LDH has been assembled with Bovine bone biochar to observe its capacity for caffeine removal from aqueous media (Meili et al., 2019). Bone-biochar was added at the co-precipitation stage of the synthesis process of the lamellar hydroxides (LDHs). An optimum of 26 mg/g adsorption capacity was achieved in this study (dos Santos Lins et al., 2019). High adsorption capacities were reported for calcined Mg-Al-LDH composite with bagasse biomass to remove tetracycline antibiotic from aqueous media; however, details presented were not enough for the calculation of partition coefficient in order to compare the performance (Tan et al., 2016c). In summary, only a limited number of studies are published in the literature on the potential of LDH assembled biochar for the removal of pharmaceuticals and personal care products, which are a group of emerging contaminants.

3.5. Removal rates

Another important aspect of adsorption is sorption kinetics, which provides information about the adsorption rate, equilibrium time and effectiveness of the adsorbent (Bonilla-Petriciolet et al., 2017). A good adsorbent should have fast kinetics and good adsorption capacity. Most of the composites indicated the best fit for pseudo second order, pseudo first order and intra-particle diffusion models with varying removal rates (Bolbol et al., 2019; Wang et al., 2020; Zhang et al., 2019). Removal rates are listed in Table 2. In general, LDH assisted biochar composites demonstrated adsorption process with two different adsorption stages; a fast adsorption stage in the beginning (due to the abundance of adsorption sites during the initial stage of adsorption), and a slow adsorption at a later stage (due to saturation of adsorption sites), (Jiang et al., 2019; Tan et al., 2016c; Zhang et al., 2013). Experiments in literature were conducted for 24 h however, predominantly, adsorption reached equilibrium within first 4 h irrespective of the composite or contaminant examined (dos Santos Lins et al., 2019; Huang et al., 2019; Wang et al., 2018; Xue et al., 2016). Comparison of kinetic data in the literature showed close fit to pseudo-second-order model, which describes chemisorption process is predominantly responsible for adsorption of contaminants (Meili et al., 2019; Zhang et al., 2019). Particularly for phosphate, the kinetic modeling data depicted film diffusion as the controlling factor for the rate of phosphate adsorption rather than pore diffusion in LDH assisted rice husk derived biochar composite basically due to the effective diffusion coefficient values ranged in between 10^{-6} to 10^{-8} cm^2/s, demonstrating high affinity of composite to phosphate (Lee et al., 2019).

3.6. Regeneration of LDH-biochar composites

An important feature of an adsorbent is its environmentally friendly regeneration, so it can be reused for multiple times in water treatment, making the process economically feasible. Efficient regeneration of multiple adsorbent usage of LDH assembled biochar composite after saturation may cause a reduction in adsorption capacity. Pure methanol and NaCl solutions (0.5 mol/L) were used as desorption agents to test the reusability of Mg-Al-LDH tailored bovine bone-char composite for remediation of caffeine even after six successful adsorption-desorption cycles (dos Santos Lins et al., 2019). Authors concluded that the regeneration was more effective with methanol than NaCl due to the high affinity of caffeine with methanol; thus, separation from the solid surface was effective (dos Santos Lins et al., 2019; Zhang et al., 2018a). LDH decorated magnetic biochar composite showed surface co-precipitation of Pb$_3$(CO$_3$)$_2$(OH)$_2$ after desorption with 2 mol/L NaOH (Jia et al., 2019). The composite was found to be effective even after reusing upto 5 cycles. Corroborative results demonstrated high

adsorption and reusability of rice husk biochar-LDH composite for Pb (II) removal after 3 cycles (Yu et al., 2018). In another study, only 78% of phosphate was desorbed with 0.5 M NaOH due to inner-sphere surface complexation in case of rice-husk biochar with calcined Mg-Al-LDHs (Lee et al., 2019). However, plant-based magnetic biochar composite with Mg-Al-LDHs showed lower adsorption capacity for phosphate at elevated pHs indicating the potential use of alkaline media with 0.1 M NaOH for the regeneration of the composites and a decrease of 51% of phosphate removal was observed at the end of the fifth cycle (Cui et al., 2019). Desorption capacity of Ni-Fe-LDHs was assessed with 0.1 M NaOH solution for As(V)-loaded composite indicated a complete recovery of the adsorbent at the end of the second cycle, wherein only 3% of As(V) was retained onto the adsorbent due to the inner-sphere complexation (Wang et al., 2016).

4. Removal mechanisms

The mechanisms of adsorptive removal of environmental contaminants using LDH assembled biochar composite have been reported in various studies (Cui et al., 2019; Wang et al., 2016; Zhang et al., 2018b). The changes that occurred before and after the sorption of pollutants to the composites have been analyzed using spectroscopic techniques such as FTIR, XRD, and BET analyses to elucidate the mechanism of adsorption onto the LDH-biochar composites. A brief schematic illustration of different pollutants onto a generalized form of LDH-biochar composites is shown in Fig. 2. It was speculated that the specific surface area of the LDH tailored biochar composite is generally lower than that of the biochar, functionalized and intercalated with LDH to create a platform for the adsorption of pollutants with the LDHs. The anionic species in the interlamellar region of LDHs are highly exchangeable, and the absence of cross-linkages between the layers of lamellar hydroxides provide for the layers to expand or contract, which gives an added advantage for the adsorbent to accommodate adsorbates (Bukhtiyarova, 2019). Anionic species can interchange organic or inorganic, oxo-anions, toxic pollutants, and various ionic moieties of organic pollutants (De Roy et al., 2001; Williams et al., 2006).

Removal of organic pollutants, such as antibiotics onto LDH-biochar composites follows a different route compared to inorganic nutrients and metal ions. Suggested interactions for the adsorption of tetracycline antibiotic, as studied by Tan et al. (2016c are π-π electron donor-acceptor interactions and hydrogen bonding. Tetracycline adsorption by calcined Mg-Al-LDH-biochar composite is attributed to the active sites of the surface functional groups of the composite, wherein the infrared spectra suggested the formation of hydrogen bonds between hydroxyl-group from the composite and the amino-group from the tetracycline (Chen et al., 2009). The absorption bands of OH group stretching vibrations and CO group bending vibrations shifted significantly after calcined Mg-Al-LDH-biochar is treated with the antibiotics, indicating the formation of hydrogen bonds through the available hydroxyl group and amino group, present in the tetracycline antibiotics (Tan et al., 2016c; Yu et al., 2017). This result is also consistent with the result obtained from the XRD spectra. During the reconstruction of the composite through calcination and further treatment with the antibiotic causes OH groups to be released. Tetracycline exists as anionic species at elevated pH and get further intercalated in the interlayer of the LDH consisting of carbonate and hydroxide groups. Moreover, π-π bonding is revealed through the C═C stretching, observed in the FTIR spectra, which suggests an interaction between the electron-deficient benzene ring of the tetracycline and the composite surface (Tan et al., 2016c). More mechanistic studies are however, needed with complex organic pollutants to understand the removal mechanisms of such pollutants by LDH/biochar composites.

Zhang et al. (2018b reported the synthesis of Mg-Fe-LDH-biochar composite and assessed its efficiency for co-sorption of inorganic nitrogen and heavy metals. Surface precipitation was suggested as the predominant route for the adsorption of Pb(II) and Cd(II). This was
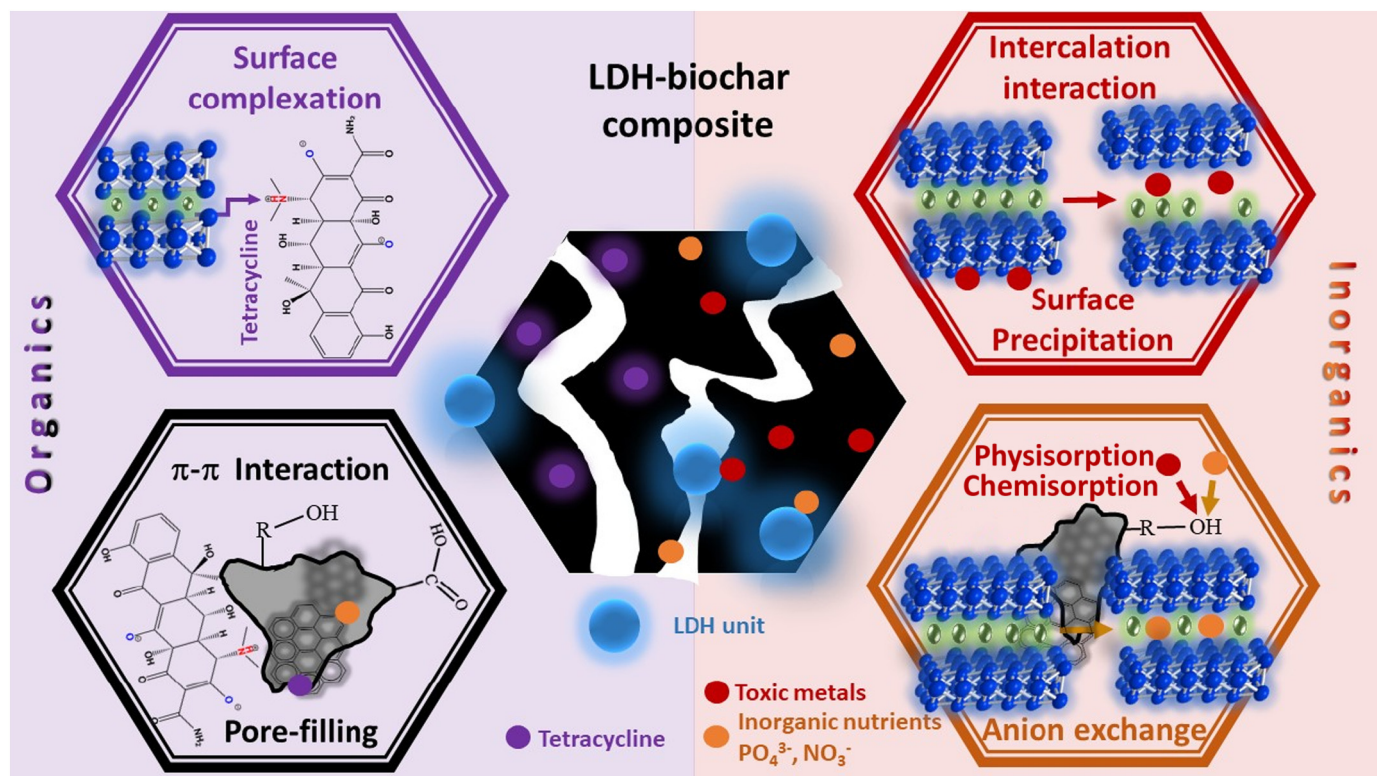
Fig. 2. Schematic illustrations of predominant mechanism for pollutant adsorption on LDH-biochar composite.

supported by the analysis, provided by the infrared spectra wherein carbonate stretching vibrations were significant in the spectra and corroborated with the XRD spectra, suggesting the formation of carbonates after treatment with Pb(II) and Cd(II). Formation of $Cu_2(OH)_3Cl$, Cu precipitates and $Pb_3(CO_3)_2(OH)_2$, lead carbonate precipitation was also assessed by the XRD spectra on treated Mg-Fe-LDH-biochar composite. Surface complexation is another contributing factor, where COO/OH functional groups on the biochar interact with Zn(II) and Ni(II) ions from the liquid phase. This route is not fully supported by a corroborative data in the study, however, isomorphic substitution through the exchange of the available cations, in this case, Mg(II), replaced by heavy metals Cu(II), Ni(II) and Pb(II) was well observed (Rojas, 2016; Zhang et al., 2018b). Thus, surface precipitation on the LDH's surface is the dominant route, compared with surface complexation on the biochar surface for the adsorption of heavy metals onto Mg-Fe-LDH-biochar composite (Zhang et al., 2018b). The surface complexation of As(V) on biochar surface and Ni-Fe-LDH-biochar composite was also investigated by Wang et al. (2016. As(V) complexation with hydroxyl-group on the biochar surface was reported unlikely due to the lower adsorption capacity, obtained from the pristine biochar, however, As(V)-LDH-biochar, through hydroxyl complexation, was found to be the most suitable route for the adsorption process (Wang et al., 2016).

Intercalation is also the predominant interaction for anionic pollutants. As studied by Jiang et al. (2019), comparison of XRD spectrum before and after phosphate adsorption showed that the interlayer spacing significantly increased after adsorption. Based on the spectrum, the assumption was made that the PO_4^{3-} intercalated into the ZnAl-LDH banana straw biochar through the interlayer channel in a perpendicular manner, thereby widening the d-spacing after phosphate adsorption (Jiang et al., 2019). This analysis is consistent with the results obtained for FTIR where a very distinct P—O stretching and bending vibration absorption peaks were observed, thereby, the interlamellar OH groups were replaced effectively by the adsorbed phosphate. Hydrogen bonding interactions were also postulated from the XPS spectra where the change in oxidation state of O-C=O bonds before and after phosphate

adsorption was noticed in the C1s XPS spectra. The change indicated an interaction between C—O and HPO_4^{2-} through the convolution obtained from O1s and Al2p/Zn2p spectra forming a Zn-O-P bonds. Wherein, Zn is attributed to come from the mineral phase $Zn_3(PO_4)_2.4H_2O$ which was also corroborated with the results obtained from XRD spectra (Jiang et al., 2019; Sheng et al., 2019).

Solution pH also has a significant role in the adsorption process that affects both the surface charges of the adsorbents and the functional groups pertaining to the adsorbents. Variable charges in the media provide surface sites for non-specific adsorption (Ramanayaka et al., 2020). At acidic conditions, more hydronium ions are available on the adsorbent surface, becoming more positively charged, which favors the adsorption of negatively charged species (Tan et al., 2016b). This is in codependence with the zero-point charge of the adsorbent, which also differs from the changes in the alkalinity and acidity of the surrounding media. Ni-Fe-LDH-biochar composite was studied for the removal of As(V), which possessed a net positive charge due to the protonation at the optimum experimental pH of 7.5, though the zero-point charge of the LDH-biochar composite was 10. At the incremented adsorption of As(V) at lower pH, it was speculated to account for the hydroxyl-group from the LDHs, causing protonation forming inner-sphere complexes with the surface (Wang et al., 2016). Similar studies were carried out by Cui et al. (2019, where the effect of co-existing ions on phosphate removal was reported by Mg-Al-LDH-biochar composite. Anions did not show a competing effect thereby, suggesting inner-sphere complexation with hydroxides, forming metal hydroxides complexes on the composite surface.

5. Conclusions and future perspectives

Incorporating LDH into biochar has proven to be beneficial for the removal of diverse pollutants from aqueous media. LDH-biochar hybrid composites have been applied for various contaminants removal from water including many different toxic metals, pharmaceuticals, inorganic nutrients and dyes. Majority of the studies are focused on phosphate

and Pb(II) removal, whereas limited attention was given for the removal of dyes, pharmaceuticals and personal care products. From the reviewed literature, it is evident that LDHs-biochar composites have shown promising results in the removal of various aquatic pollutants compared to other adsorbents. The most predominant adsorption mechanisms for different pollutants include electrostatic attraction and intercalation interactions, hydrogen bonding, and chemical bonding (complexation and/or precipitation). However, interaction of both pristine biochar and pristine LDH in water for different contaminants consist of different parameters and the methods utilized are distinct for different studies, thus, a direct comparison is impossible. The partition coefficient values, which indicate performance of adsorbents, seemed low for the major adsorbent reviewed here. High partition coefficients were reported for toxic metals; Pb, Cu, Ni, Zn and Cd as 1100, 19, 5, 4 and 4 L/g. Among other contaminants, phosphate demonstrated high partition coefficient values, i.e. 6 g/L. Although limited studies have focused on the removal of organic pollutants using biochar composites, but promising have been reported.

Interestingly, most studies have examined the co-existence of other anions and cations. However, no attention was paid for the adsorption of persistent organic pollutants or agrochemicals (pesticides and herbicides) by the LDH tailored biochar composites. From the literature reviewed, Mg/Fe-LDH biochar was the sole study reporting the column experiments to test the uptake of divalent cationic species, in the amended soils (Zhang et al., 2018b). Further studies need to be showcased for the efficiency of these composites through performing more soil-column experiments for the identification of pollutants.

Studies need to be conducted on the effect of pyrolysis temperature and the source of biomass for biochar production to provide the favorable support for LDHs active sites. Moreover, few raw materials and functional biochar materials may contain toxic elements that can cause secondary pollution to the water environment after water treatment. Thus, the stability of the synthesized LDH-biochar composites needs to be considered in actual wastewater treatment plants. Newer strategies for developing the composites from varied biochar sources i.e. municipal waste, forest residues apart from crop residues, should also be further explored. Incongruent with the biochar studies with LDHs, surface charge, and Boehm titrations needed to be exemplified for the composites to understand the factors influencing the mechanisms it undertakes to uptake the pollutants.

Similarly, batch adsorption studies should be further extended at different temperatures derived biochars for composite preparation in order to assess the influence of surface functional groups of biochar in the adsorption process. As many studies are based on batch adsorption, hence, column studies are essential in order to assess the flow parameters. Further, binary and tertiary systems for the understanding of competition of contaminants are also inevitable before field scale settings. Novel research is vital to demonstrate the cost effectiveness of LDH tailored biochar composites through cost-benefit analysis for its upscaling. Also, practical applications of LDHs-biochar composites should be tested in pilot-scale with real wastewater containing multi-pollutants.

CRediT authorship contribution statement

Meththika Vithanage: Conceptualization, Funding acquisition, Writing - review & editing. **Ahmed Ashiq:** Formal analysis, Writing - original draft. **Sammani Ramanayaka:** Formal analysis, Writing - original draft. **Amit Bhatnagar:** Writing - review & editing.

Declaration of competing interest

We hereby certify that there is no conflict of interest among authors.

Acknowledgments

Appendix A. Supplementary data

Supplementary data to this article can be found online at https://doi.org/10.1016/j.scitotenv.2020.139718.

References

Ahmad, M., Rajapaksha, A.U., Lim, J.E., Zhang, M., Bolan, N., Mohan, D., et al., 2014. Biochar as a sorbent for contaminant management in soil and water: a review. Chemosphere 99, 19–33.

Aksu, Z., Tatlı, A.İ., Tunç, Ö., 2008. A comparative adsorption/biosorption study of Acid Blue 161: effect of temperature on equilibrium and kinetic parameters. Chem. Eng. J. 142, 23–39.

Alagha, O., Manzar, M.S., Zubair, M., Anil, I., Mu'azu, N.D., Qureshi, A., 2020. Comparative adsorptive removal of phosphate and nitrate from wastewater using biochar-MgAl LDH nanocomposites: coexisting anions effect and mechanistic studies. Nanomaterials 10, 336.

Ashiq, A., Adassooriya, N.M., Sarkar, B., Rajapaksha, A.U., Ok, Y.S., Vithanage, M., 2019. Municipal solid waste biochar-bentonite composite for the removal of antibiotic ciprofloxacin from aqueous media. J. Environ. Manag. 236, 428–435.

Bolbol, H., Fekri, M., Hejazi-Mehrizi, M., 2019. Layered double hydroxide–loaded biochar as a sorbent for the removal of aquatic phosphorus: behavior and mechanism insights. Arab. J. Geosci. 12, 503.

Bonilla-Petriciolet, A., Mendoza-Castillo, D.I., Reynel-Ávila, H.E., 2017. Adsorption Processes for Water Treatment and Purification. Springer International Publishing, Cham.

Bukhtiyarova, M.V., 2019. A review on effect of synthesis conditions on the formation of layered double hydroxides. J. Solid State Chem. 269, 494–506.

Chen, S., Xu, Z.P., Zhang, Q., Lu, G.Q.M., Hao, Z.P., Liu, S., 2009. Studies on adsorption of phenol and 4-nitrophenol on MgAl-mixed oxide derived from MgAl-layered double hydroxide. Sep. Purif. Technol. 67, 194–200.

Cui, Q., Jiao, G., Zheng, J., Wang, T., Wu, G., Li, G., 2019. Synthesis of a novel magnetic Caragana korshinskii biochar/Mg–Al layered double hydroxide composite and its strong adsorption of phosphate in aqueous solutions. RSC Adv. 9, 18641–18651.

Daud, M., Hai, A., Banat, F., Wazir, M.B., Habib, M., Bharath, G., et al., 2019. A review on the recent advances, challenges and future aspect of layered double hydroxides (LDH) – containing hybrids as promising adsorbents for dyes removal. J. Mol. Liq. 288, 110989.

De Roy, A., Forano, C., Besse, J.P., 2001. Layered Double Hydroxides: Synthesis and Post-synthesis Modification. Layered Double Hydroxides: Present and Future. pp. 1–39.

dos Santos Lins, P.V., Henrique, D.C., Ide, A.H., de Paivae Silva Zanta, C.L., Meili, L., 2019. Evaluation of caffeine adsorption by MgAl-LDH/biochar composite. Environ. Sci. Pollut. Res. 26, 31804–31811.

El Gaini, L., Lakraimi, M., Sebbar, E., Meghea, A., Bakasse, M., 2009. Removal of indigo carmine dye from water to Mg–Al–CO3-calcined layered double hydroxides. J. Hazard. Mater. 161, 627–632.

Gholami, P., Dinpazhoh, L., Khataee, A., Hassani, A., Bhatnagar, A., 2020a. Facile hydrothermal synthesis of novel Fe-Cu layered double hydroxide/biochar nanocomposite with enhanced sonocatalytic activity for degradation of cefazolin sodium. J. Hazard. Mater. 381, 120742.

Gholami, P., Khataee, A., Soltani, R.D.C., Dinpazhoh, L., Bhatnagar, A., 2020b. Photocatalytic degradation of gemifloxacin antibiotic using Zn-Co-LDH@biochar nanocomposite. J. Hazard. Mater. 382, 121070.

He, X., Qiu, X., Hu, C., Liu, Y., 2018. Treatment of heavy metal ions in wastewater using layered double hydroxides: a review. J. Dispers. Sci. Technol. 39, 792–801.

Huang, D., Liu, C., Zhang, C., Deng, R., Wang, R., Xue, W., et al., 2019. Cr(VI) removal from aqueous solution using biochar modified with Mg/Al-layered double hydroxide intercalated with ethylenediaminetetraacetic acid. Bioresour. Technol. 276, 127–132.

Jia, Y., Zhang, Y., Fu, J., Yuan, L., Li, Z., Liu, C., et al., 2019. A novel magnetic biochar/MgFe-layered double hydroxides composite removing Pb2+ from aqueous solution: isotherms, kinetics and thermodynamics. Colloids Surf. A Physicochem. Eng. Asp. 567, 278–287.

Jiang, Y.-H., Li, A.-Y., Deng, H., Ye, C.-H., Li, Y., 2019. Phosphate adsorption from wastewater using ZnAl-LDO-loaded modified banana straw biochar. Environ. Sci. Pollut. Res. 26, 18343–18353.

Lee, S.Y., Choi, J.-W., Song, K.G., Choi, K., Lee, Y.J., Jung, K.-W., 2019. Adsorption and mechanistic study for phosphate removal by rice husk-derived biochar functionalized with Mg/Al-calcined layered double hydroxides via co-pyrolysis. Compos. Part B 176, 107209.

Li, R., Wang, J.J., Zhou, B., Awasthi, M.K., Ali, A., Zhang, Z., et al., 2016. Enhancing phosphate adsorption by Mg/Al layered double hydroxide functionalized biochar with different Mg/Al ratios. Sci. Total Environ. 559, 121–129.

Mandal, S., Pu, S., Adhikari, S., Ma, H., Kim, D.-H., Bai, Y., et al., 2020. Progress and future prospects in biochar composites: application and reflection in the soil environment. Crit. Rev. Environ. Sci. Technol. 1–53.

Meili, L., Lins, P.V., Zanta, C.L.P.S., Soletti, J.I., Ribeiro, L.M.O., Dornelas, C.B., et al., 2019. MgAl-LDH/biochar composites for methylene blue removal by adsorption. Appl. Clay Sci. 168, 11–20.

Mishra, G., Dash, B., Pandey, S., 2018. Layered double hydroxides: a brief review from fundamentals to application as evolving biomaterials. Appl. Clay Sci. 153, 172–186.

Mohapatra, L., Parida, K., 2016. A review on the recent progress, challenges and perspective of layered double hydroxides as promising photocatalysts. J. Mater. Chem. A 4, 10744–10766.

Ok, Y.S., Chang, S.X., Gao, B., Chung, H.-J., 2015. SMART biochar technology—a shifting paradigm towards advanced materials and healthcare research. Environmental Technology & Innovation 4, 206–209.

Peiris, C., Gunatilake, S.R., Mohan, D., Vithanage, M., 2017. Biochar based removal of antibiotic sulfonamides and tetracyclines in aquatic environments: a critical review. Bioresour. Technol. 246, 150–159.

Peiris, C., Gunatilake, S.R., Wewalwela, J.J., Vithanage, M., 2019. Chapter 11 - biochar for sustainable agriculture: nutrient dynamics, soil enzymes, and crop growth. In: Ok, Y.S., Tsang, D.C.W., Bolan, N., Novak, J.M. (Eds.), Biochar from Biomass and Waste. Elsevier, pp. 211–224.

Premarathna, K.S.D., Rajapaksha, A.U., Adassoriya, N., Sarkar, B., Sirimuthu, N.M.S., Cooray, A., et al., 2019a. Clay-biochar composites for sorptive removal of tetracycline antibiotic in aqueous media. J. Environ. Manag. 238, 315–322.

Premarathna, K.S.D., Rajapaksha, A.U., Sarkar, B., Kwon, E.E., Bhatnagar, A., Ok, Y.S., et al., 2019b. Biochar-based engineered composites for sorptive decontamination of water: a review. Chem. Eng. J. 372, 536–550.

Rajapaksha, A.U., Chen, S.S., Tsang, D.C.W., Zhang, M., Vithanage, M., Mandal, S., et al., 2016. Engineered/designer biochar for contaminant removal/immobilization from soil and water: potential and implication of biochar modification. Chemosphere 148, 276–291.

Ramanayaka, S., Sarkar, B., Cooray, A.T., Ok, Y.S., Vithanage, M., 2020. Halloysite nanoclay supported adsorptive removal of oxytetracycline antibiotic from aqueous media. J. Hazard. Mater. 384, 121301.

Rojas, R., 2016. Effect of particle size on copper removal by layered double hydroxides. Chem. Eng. J. 303, 331–337.

Sheng, T., Zhang, Z., Hu, Y., Tao, Y., Zhang, J., Shen, Z., et al., 2019. Adsorption of phosphorus by using magnetic Mg–Al-, Zn–Al- and Mg–Fe-layered double hydroxides: comparison studies and adsorption mechanism. Environ. Sci. Pollut. Res. 26, 7102–7114.

de Souza dos Santos, G.E., Ide, A.H., Duarte, J.L.S., McKay, G., Silva, A.O.S., Meili, L., 2020. Adsorption of anti-inflammatory drug diclofenac by MgAl/layered double hydroxide supported on Syagrus coronata biochar. Powder Technol. 364, 229–240.

Sun, L., Wan, S., Luo, W., 2013. Biochars prepared from anaerobic digestion residue, palm bark, and eucalyptus for adsorption of cationic methylene blue dye: characterization, equilibrium, and kinetic studies. Bioresour. Technol. 140, 406–413.

Takehira, K., 2017. Recent development of layered double hydroxide-derived catalysts —rehydration, reconstitution, and supporting, aiming at commercial application—. Appl. Clay Sci. 136, 112–141.

Tan, X.-F., Liu, Y.-G., Gu, Y.-L, Liu, S.-B., Zeng, G.-M., Cai, X., et al., 2016a. Biochar pyrolyzed from MgAl-layered double hydroxides pre-coated ramie biomass (Boehmeria nivea (L.) Gaud.): characterization and application for crystal violet removal. J. Environ. Manag. 184, 85–93.

Tan, X.-F., Liu, Y.-G., Gu, Y.-L, Xu, Y., Zeng, G.-M., Hu, X.-J., et al., 2016b. Biochar-based nano-composites for the decontamination of wastewater: a review. Bioresour. Technol. 212, 318–333.

Tan, X., Liu, S., Liu, Y., Gu, Y., Zeng, G., Cai, X., et al., 2016c. One-pot synthesis of carbon supported calcined-Mg/Al layered double hydroxides for antibiotic removal by slow pyrolysis of biomass waste. Sci. Rep. 6, 39691.

Tan, Y., Yin, X., Wang, C., Sun, H., Ma, A., Zhang, G., et al., 2019. Sorption of cadmium onto Mg-Fe Layered Double Hydroxide (LDH)-Kiwi branch biochar. Environmental Pollutants and Bioavailability 31, 189–197.

Theiss, F.L., Ayoko, G.A., Frost, R.L., 2016. Synthesis of layered double hydroxides containing Mg2+, Zn2+, Ca2+ and Al3+ layer cations by co-precipitation methods—a review. Appl. Surf. Sci. 383, 200–213.

Vithanage, M., Herath, I., Joseph, S., Bundschuh, J., Bolan, N., Ok, Y.S., et al., 2017. Interaction of arsenic with biochar in soil and water: a critical review. Carbon 113, 219–230.

Wan, S., Wang, S., Li, Y., Gao, B., 2017. Functionalizing biochar with Mg-Al and Mg-Fe layered double hydroxides for removal of phosphate from aqueous solutions. J. Ind. Eng. Chem. 47, 246–253.

Wang, S., Gao, B., Li, Y., Zimmerman, A.R., Cao, X., 2016. Sorption of arsenic onto Ni/Fe layered double hydroxide (LDH)-biochar composites. RSC Adv. 6, 17792–17799.

Wang, T., Li, C., Wang, C., Wang, H., 2018. Biochar/MnAl-LDH composites for Cu (II) removal from aqueous solution. Colloids Surf. A Physicochem. Eng. Asp. 538, 443–450.

Wang, H., Wang, S., Chen, Z., Zhou, X., Wang, J., Chen, Z., 2020. Engineered biochar with anisotropic layered double hydroxide nanosheets to simultaneously and efficiently capture Pb2+ and CrO42− from electroplating wastewater. Bioresour. Technol. 306, 123118.

Williams, G.R., Khan, A.I., O'Hare, D., 2006. Mechanistic and kinetic studies of guest ion intercalation into layered double hydroxides using time-resolved, in-situ X-ray powder diffraction. Layered Double Hydroxides. Springer, pp. 161–192.

Xiang, W., Zhang, X., Chen, J., Zou, W., He, F., Hu, X., et al., 2020. Biochar technology in wastewater treatment: a critical review. Chemosphere 126539.

Xu, R.-K., Xiao, S.-C., Yuan, J.-H., Zhao, A.-Z., 2011. Adsorption of methyl violet from aqueous solutions by the biochars derived from crop residues. Bioresour. Technol. 102, 10293–10298.

Xue, L., Gao, B., Wan, Y., Fang, J., Wang, S., Li, Y., et al., 2016. High efficiency and selectivity of MgFe-LDH modified wheat-straw biochar in the removal of nitrate from aqueous solutions. J. Taiwan Inst. Chem. Eng. 63, 312–317.

Yan, K., Wu, G., Jin, W., 2016. Recent advances in the synthesis of layered, double-hydroxide-based materials and their applications in hydrogen and oxygen evolution. Energy Technology 4, 354–368.

Yang, F., Zhang, S., Sun, Y., Tsang, D.C.W., Cheng, K., Ok, Y.S., 2019. Assembling biochar with various layered double hydroxides for enhancement of phosphorus recovery. J. Hazard. Mater. 365, 665–673.

Yao, Y., Gao, B., Fang, J., Zhang, M., Chen, H., Zhou, Y., et al., 2014. Characterization and environmental applications of clay–biochar composites. Chem. Eng. J. 242, 136–143.

Yu, S., Wang, X., Chen, Z., Wang, J., Wang, S., Hayat, T., et al., 2017. Layered double hydroxide intercalated with aromatic acid anions for the efficient capture of aniline from aqueous solution. J. Hazard. Mater. 321, 111–120.

Yu, J., Zhu, Z., Zhang, H., Qiu, Y., Yin, D., 2018. Mg–Fe layered double hydroxide assembled on biochar derived from rice husk ash: facile synthesis and application in efficient removal of heavy metals. Environ. Sci. Pollut. Res. 25, 24293–24304.

Zhang, M., Gao, B., Yao, Y., Inyang, M., 2013. Phosphate removal ability of biochar/MgAl-LDH ultra-fine composites prepared by liquid-phase deposition. Chemosphere 92, 1042–1047.

Zhang, J., Lu, M., Wan, J., Sun, Y., Lan, H., Deng, X., 2018a. Effects of pH, dissolved humic acid and Cu2+ on the adsorption of norfloxacin on montmorillonite-biochar composite derived from wheat straw. Biochem. Eng. J. 130, 104–112.

Zhang, L., Tang, S., Jiang, C., Jiang, X., Guan, Y., 2018b. Simultaneous and efficient capture of inorganic nitrogen and heavy metals by polyporous layered double hydroxide and biochar composite for agricultural nonpoint pollution control. ACS Appl. Mater. Interfaces 10, 43013–43030.

Zhang, Z., Yan, L., Yu, H., Yan, T., Li, X., 2019. Adsorption of phosphate from aqueous solution by vegetable biochar/layered double oxides: fast removal and mechanistic studies. Bioresour. Technol. 284, 65–71.

Zhao, M., Zhao, Q., Li, B., Xue, H., Pang, H., Chen, C., 2017. Recent progress in layered double hydroxide based materials for electrochemical capacitors: design, synthesis and performance. Nanoscale 9, 15206–15225.